



Molecular Structures and Redox Properties of Homoleptic Aluminum(III) Complexes with Azobisphenolate (azp) Ligands

Takahashi, Kazuyuki

Noguchi, Takumi

Ueda, Keiji

Miyawaki, Atsuhiro

Murata, Suguru

(Citation)

Inorganics, 10(6):84

(Issue Date)

2022-06

(Resource Type)

journal article

(Version)

Version of Record

(Rights)

© 2022 by the authors. Licensee MDPI, Basel, Switzerland.

This article is an open access article distributed under the terms and conditions of the Creative Commons Attribution (CC BY) license (<https://creativecommons.org/licenses/by/4.0/>).


(URL)

<https://hdl.handle.net/20.500.14094/90009462>



Article

Molecular Structures and Redox Properties of Homoleptic Aluminum(III) Complexes with Azobisphenolate (azp) Ligands

Kazuyuki Takahashi , Takumi Noguchi, Keiji Ueda, Atsuhiko Miyawaki and Suguru Murata

Department of Chemistry, Graduate School of Science, Kobe University, 1-1 Rokkodai, Nada-ku, Kobe 657-8501, Japan; nogutaku.789@gmail.com (T.N.); uediji3105@gmail.com (K.U.); a.miyawaki0205@gmail.com (A.M.); murata.sgr@gmail.com (S.M.)

* Correspondence: ktaka@crystal.kobe-u.ac.jp; Tel.: +81-78-803-5691

Abstract: To elucidate the oxidation behavior of the 2,2'-azobisphenolate (azp) ligand, a series of homoleptic 1:2 Al^{III} complexes of four azp derivatives (L1) with 5,5'-dichloro-, 5,5'-dimethyl-, 5,5'-di-*t*-butyl-, 3,3',5,5'-tetramethyl-substituents and of one imino derivative (L2) were synthesized and obtained as TPP[Al(L)₂]₂·solvent (TPP = tetraphenylphosphonium ion). The X-ray crystal structure analyses showed that the two ONO-tridentate ligands were meridionally coordinated to a central Al^{III} ion in an almost perpendicular manner to give a homoleptic octahedral coordination structure in all the Al^{III} complexes. The proton nuclear magnetic resonance spectra suggested that all the Al^{III} complexes retained the homoleptic coordination structure in solution. From the cyclic voltammetry measurements in dichloromethane solutions, all the Al^{III} complexes with the azp ligands showed two partially reversible oxidation waves, and an additional reversible or partially reversible reduction wave. The substitution effects on the first oxidation and reduction peak potentials were revealed in the Al^{III} complexes with the azp ligands. On the other hand, the imino complex showed a partially reversible oxidation wave accompanying a film deposition. The density functional theory (DFT) calculations indicated that the molecular orbital (MO) coefficients of the frontier MOs in the Al^{III} complexes were present on the ligands and were absent on the Al^{III} ion. These results confirmed that the azp ligands are susceptible to oxidation and can give a relatively stable oxidation species depending upon substituent effects.

Keywords: azobisphenolate ligand; aluminum complex; redox-active ligand; crystal structure; redox property; DFT calculation



Citation: Takahashi, K.; Noguchi, T.; Ueda, K.; Miyawaki, A.; Murata, S. Molecular Structures and Redox Properties of Homoleptic Aluminum(III) Complexes with Azobisphenolate (azp) Ligands. *Inorganics* **2022**, *10*, 84. <https://doi.org/10.3390/inorganics10060084>

Academic Editor: Wolfgang Linert

Received: 4 April 2022

Accepted: 14 June 2022

Published: 16 June 2022

Publisher's Note: MDPI stays neutral with regard to jurisdictional claims in published maps and institutional affiliations.



Copyright: © 2022 by the authors. Licensee MDPI, Basel, Switzerland. This article is an open access article distributed under the terms and conditions of the Creative Commons Attribution (CC BY) license (<https://creativecommons.org/licenses/by/4.0/>).

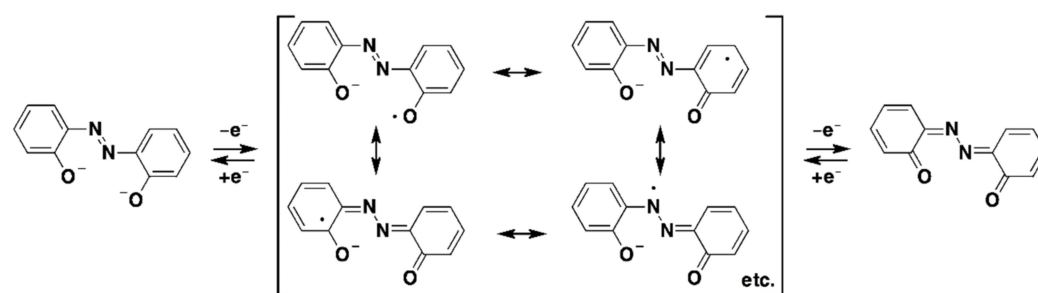
1. Introduction

Redox-active ligands are relatively easily oxidized or reduced molecules that can be coordinated with various metal ions. The electronic state of redox-active ligands can be switched by not only an electric potential but also by interactions with chemical substances. In particular, the interactions with a coordinated metal ion can create various exotic phenomena such as valence tautomerism in metal dioxolene complexes [1], electron-transfer-induced ferromagnetism in paddle-wheel ruthenium complexes with tetracyanoquinodimethane (TCNQ) derivatives [2], and extremely stable metallic state and various metal-insulator transitions in copper *N,N'*-dicyanoquinodimines (DCNQIs) complexes [3]. These intriguing phenomena originate from either charge transfer, electron transfer, or orbital interaction between a metal ion and redox-active ligand. Because the electron transfer can induce spin-state switching and/or the change in magnetic exchange coupling and electric polarization involved in metal ions and redox-active ligands, these complexes can afford magnetic and dielectric switching materials.

2,2'-Azobisphenol (H₂azp) is one of the azo dyes known as intense coloring and/or fluorometric reagents that can quantitatively analyze for specific ions such as magnesium [4–7], aluminum [4,8–10], and gallium [4,8,9]. The molecular structures of homoleptic 1:2 Cr^{III}

and Co^{III} complexes with azp derivatives were extensively studied by Schetty [11–16]. The meridional ONO-tridentate coordination to metal ions was confirmed by the crystal structure analysis for homoleptic 1:2 Cr^{III} [17] and Mn^{IV} [18] complexes with a non-substituted azp ligand. Ti^{IV} [19,20], V^{IV} [21–23], Mn^{III} [24], Co^{III} [25], Ni^{II} [26,27], Cu^{II} [28], Mo^{VI} [29], Pd^{II} [26,27], and Pt^{II} [26,27] complexes with azp derivatives have been reported as well-characterized transition metal azp complexes. Recently, we discovered the homoleptic 1:2 Fe^{III} [30,31] and heteroleptic Fe^{III} [32,33] complexes from azp derivatives exhibited gradual and abrupt spin-crossover transitions. Moreover, single-crystal-to-single-crystal transformation [34] and spin-crossover-triggered linkage isomerization involved in a pedal-like motion of the azp ligand [35] were also found in the Fe^{III} complexes with the azp derivatives. Very recently, double spin-crossover [36] and field-induced magnetic relaxation [37] were reported in homoleptic 1:2 Fe^{III} complexes with an azp ligand.

The structural formula of the deprotonated azp molecule can be regarded as the two-electron reduction form of a neutral bis-orthoquinoid compound through a monoanionic semiquinone radical (Scheme 1). Therefore, it is expected that the azp derivatives are redox-active, which can be described by a two-electron oxidation (shown as sequential one-electron oxidation steps in Scheme 1). Although there have been several reports on the electrochemical reduction of azp derivatives and their metal complexes [18,24,29,38], the electrochemical oxidation has only been reported for the Co^{III} complex with the azp derivative [25]. Since the Co^{IV} and Co^{V} complexes are known [39,40], it has never been reported whether the observed oxidation wave was centered on the metal ion or azp ligand to date.



Scheme 1. Possible redox scheme for the structural formula of 2,2'-azobisphenolate (azp) ligand.

To understand the electrochemical oxidation behavior of the azp ligand, we focused on the homoleptic 1:2 Al^{III} complexes with azp derivatives. Although an Al^{III} complex could be reduced by potassium metal under very specific conditions [41], the Al^{III} ion will clearly be redox-innocent under oxidative conditions and we anticipate no contribution from the Al^{III} ion in our study. The reported 1:1 divalent and trivalent metal complexes with azp ligands are usually insoluble in common solvents, whereas the homoleptic 1:2 Al^{III} complexes were soluble in water and organic solvents [8,10] and retained an octahedral coordination structure in the solution state [42]. The coordination with an Al^{III} ion may stabilize the dianion of azp derivatives. Therefore, the electrochemical oxidation behavior of the azp ligand itself can be clarified using the homoleptic 1:2 Al^{III} complex. Moreover, the single crystals suitable for crystal structure analysis can be obtained for homoleptic 1:2 Al^{III} complexes as many crystal structures of the homoleptic 1:2 transition metal complexes with azp derivatives have been determined. To investigate both the substitution effect on redox behavior and the steric effect of 3-substitution on metal coordination, we prepared four H_2azp derivatives ($\text{H}_2\text{L1}$) with electron-donating (methyl- and *t*-butyl-) and electron-withdrawing (chloro-) substituents at 5- and 3,5-positions using an improved synthetic procedure. We also synthesized an imino derivative ligand ($\text{H}_2\text{L2}$) to clarify the role of an azo group on redox properties. We report herein the syntheses, crystal structures, proton nuclear magnetic resonance (NMR) spectra, cyclic voltammograms, and density functional theory (DFT) calculations of the Al^{III} complexes **1** and **2** (Figure 1).

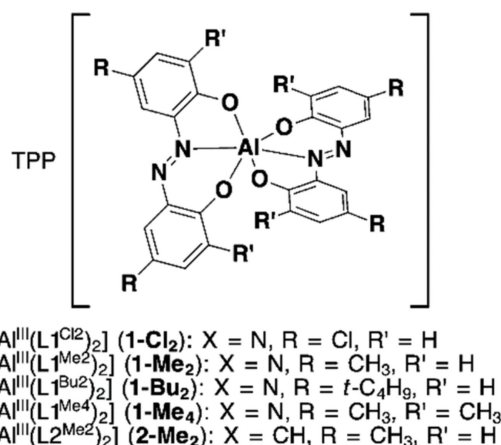


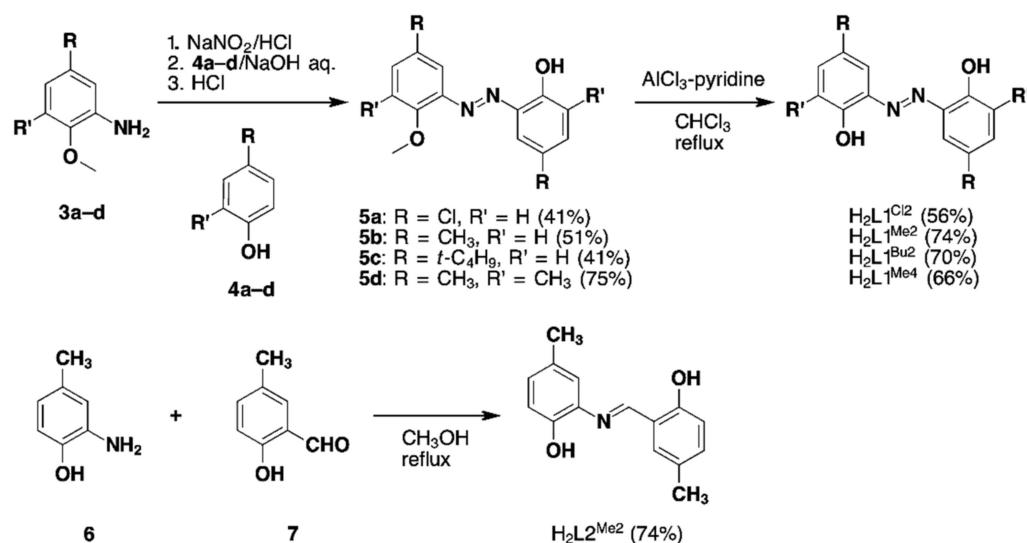
Figure 1. The molecular formula of the Al^{III} complexes **1** and **2** (TPP = tetraphenylphosphonium cation).

2. Results and Discussion

2.1. Synthesis

2.1.1. Synthesis of Substituted H₂azp Ligands (H₂L1) and Imino Derivative Ligand (H₂L2)

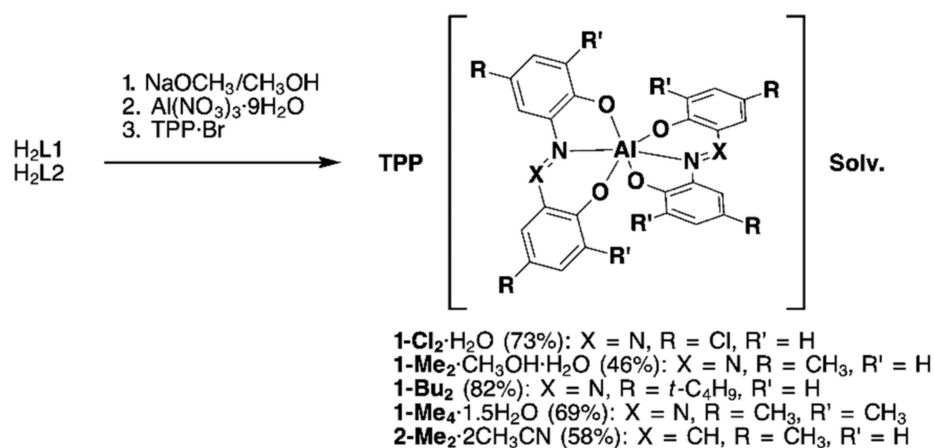
Symmetrically alkyl-substituted H₂azp derivatives were usually synthesized by the homocoupling reaction of corresponding 2-hydroxyphenyl diazonium salts in the presence of a Cu(I) complex catalyst [43]. However, this synthetic procedure usually gave relatively low yields and was unsuitable for a large-scale preparation because the reaction accompanies vigorous foaming. Because the direct azo-coupling reaction of 2-hydroxyphenyl diazonium salt sometimes failed to obtain the product, we utilized the two-step synthetic procedure for the benzene-fused azp derivative [31]. This synthetic procedure has the advantage that the symmetrical and unsymmetrical H₂azp derivatives with a position-selective substitution and electron-withdrawing substituents can be synthesized. The synthetic scheme of the ligands is shown in Scheme 2. The substituted 2-methoxyanilines **3** were converted into the diazonium salts and then reacted with an aqueous NaOH solution of 4- or 2,4-substituted phenols **4**. Deprotection of methyl group was achieved using AlCl₃-pyridine in chloroform, to give H₂azp-5,5'-Cl₂ (H₂L1^{Cl₂}) [44], H₂azp-5,5'-Me₂ (H₂L1^{Me₂}) [43], H₂azp-5,5'-*t*Bu₂ (H₂L1^{Bu₂}) [43], and H₂azp-3,3',5,5'-Me₄ (H₂L1^{Me₄}) in moderate yields. Dehydration condensation between **6** and **7** afforded the imino derivative ligand (H₂L2^{Me₂}).



Scheme 2. The synthesis scheme of ligands H₂L1 and H₂L2.

2.1.2. Synthesis of Homoleptic 1:2 Al^{III} Complexes

The homoleptic 1:2 Al^{III} complexes were prepared by the reaction of Al^{III}(NO₃)₃·9H₂O with 2 equivalents of anionic L1 or L2 ligands generated by the reaction of NaOCH₃ in methanol, followed by the addition of tetraphenylphosphonium (TPP) bromide (Scheme 3). Recrystallization in appropriate solvents gave the homoleptic Al^{III} complexes **1** and **2** as dark red needles and orange needles, respectively. The compositions of the Al^{III} complexes were confirmed by elemental analysis and crystal structure analysis described below.



Scheme 3. The synthesis scheme of the Al^{III} complexes **1** and **2**.

2.2. Crystal Structures of the Al^{III} Complexes **1** and **2**

Crystallographic data of the Al^{III} complexes **1** and **2** are listed in Table S1. The crystals except for **1-Bu₂** contained some solvent molecules. The Al^{III} complex crystals are hereafter designated as the corresponding compound number without indicating the solvent molecules. The crystal structures for **1-Me₂**, **1-Bu₂**, and **2-Me₂** belonged to the triclinic system with *P* $\bar{1}$. The crystal structures of **1-Cl₂** and **1-Me₄** belonged to the monoclinic system with *Pna*2₁ and *C2/c*, respectively. The asymmetric units for **1-Me₂**, **1-Bu₂**, and **2-Me₂** were one TPP cation and one [Al^{III}(L)₂] anion, whereas that for **1-Cl₂** was two TPP cations and two [Al^{III}(L^{Cl₂)₂] anions. The asymmetric unit for **1-Me₄** was one TPP cation and two halves of [Al^{III}(L^{Me₄)₂] anions. All the ligands in **1-Bu₂**, **1-Me₄**, and **2-Me₂** showed an orientational disorder, whereas the orientations of one ligand in **1-Me₂** and all the ligands in **1-Cl₂** were ordered. The molecular structures of the [Al^{III}(L)₂] anions in **1-Cl₂** and **1-Me₂** are shown in Figure 2. The two ligands were meridionally coordinated to a central Al^{III} ion in an almost perpendicular manner to give a homoleptic octahedral coordination structure. The substitution of the 3-position on the azp ligand with the methyl group was found to have no significant effect on metal coordination. The structural parameters of the orientationally ordered ligands in **1-Cl₂** and **1-Me₂** are listed in Table 1. The coordinate Al–O bond lengths involved in the five-membered and six-membered chelates in **1-Cl₂** and **1-Me₂** were 1.870(4)–1.890(2) and 1.843(2)–1.856(3) Å, respectively, whereas the Al–N bond lengths were 2.008(2)–2.030(4) Å. The coordinate bond lengths to the oxygen atoms were similar to those in the Co^{III} [25] complexes and shorter than those in the Fe^{III} low-spin and high-spin complexes [30] and Cu^{II} [28] complex. This trend can be explained by the relative effective cation radii of the metal ions [45]. On the other hand, the trend of the coordinate bond lengths to the nitrogen atoms is the opposite. The bond lengths of the azp ligand in **1-Cl₂** and **1-Me₂** were almost the same as those in the Co^{III} [25] and Cu^{II} [28] complexes.}}

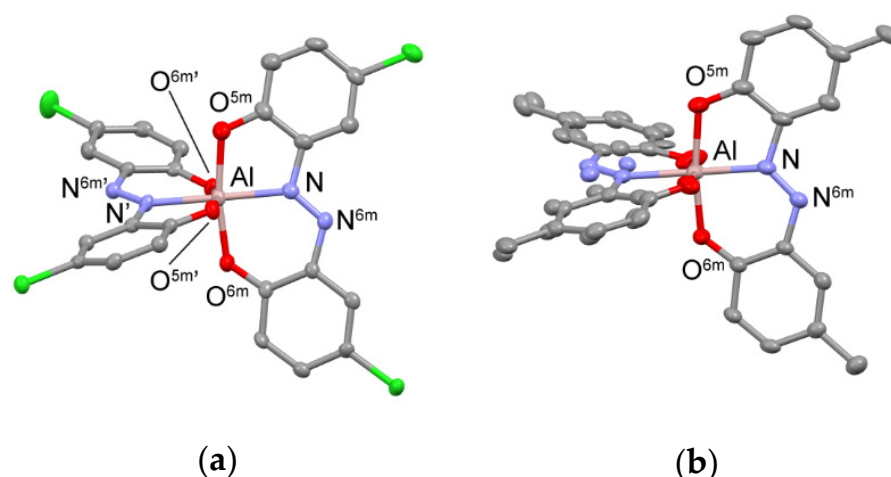


Figure 2. ORTEP drawings with a 50% probability. (a) One of the $[Al^{III}(L1^{Me2})_2]$ anions in **1-Cl₂**; (b) The $[Al^{III}(L1^{Me2})_2]$ anion in **1-Me₂**. The atoms of a minor disordered ligand are shown without bond bars.

Table 1. Coordination geometries and bonding parameters of the metal complexes with azp ligands.

Metal Ion	Al ^{III}					Co ^{III}	Cu ^{II}	Fe ^{III}	
Spin-state ^a	—					LS	—	LS	HS
Geometry ^b	Oh					Oh	Sq	Oh	Oh
R _{eff} ^c / Å	0.535					0.545	0.570	0.550	0.645
Complex	1-Cl₂					1-Me₂	Co(L)	Cu(L)	TMA[Fe(azp) ₂]
Temp.	90 K					90 K	233 K	296 K	90 K 293 K
Bond Length/Å									
M-O ^{5m}	1.882(4)	1.870(4)	1.879(3)	1.888(3)	1.890(2)	1.868(4)	1.905(4)	1.9217(14)	1.9842(18)
M-O ^{6m}	1.855(4)	1.851(3)	1.845(4)	1.856(3)	1.843(2)	1.856(4)	1.867(4)	1.8898(14)	1.9425(19)
M-N	2.020(4)	2.030(4)	2.030(4)	2.030(4)	2.008(2)	1.849(6)	1.923(6)	1.9220(15)	2.1534(18)
C-O ^{5m}	1.325(5)	1.330(6)	1.319(5)	1.325(6)	1.328(4)	1.334(8)	1.331(9)	1.312(2)	1.311(3)
C-N	1.414(6)	1.400(6)	1.417(6)	1.415(6)	1.416(3)	1.422(8)	1.405(8)	1.416(2)	1.415(3)
C-O ^{6m}	1.316(6)	1.320(5)	1.310(6)	1.314(5)	1.302(3)	1.326(8)	1.309(8)	1.319(2)	1.299(3)
C-N ^{6m}	1.384(6)	1.406(6)	1.403(6)	1.407(5)	1.391(3)	1.386(9)	1.390(9)	1.388(2)	1.391(3)
N-N ^{6m}	1.278(5)	1.276(5)	1.271(5)	1.268(5)	1.277(3)	1.266(8)	1.263(8)	1.267(2)	1.274(3)
reference	this work					ref. [25]	ref. [28]	ref. [30]	

^a LS: low-spin; HS: high-spin. ^b Oh: octahedral coordination; Sq: square-planar coordination. ^c Effective cation radii listed in Ref. [45]. ^{5m} The atom involved in a five-membered chelate. ^{6m} The atom involved in a six-membered chelate.

2.3. ¹H NMR Spectra of the Ligands and Al^{III} Complexes

¹H NMR spectra for the ligands H₂L1, H₂L2, and Al^{III} complexes **1** and **2** were measured in chloroform-*d*₆ and DMSO-*d*₆. All the Al^{III} complexes gave well-resolved spectra assigned to the single set of signals attributed to the corresponding deprotonated ligands and TPP cations. No other signals were observed in the aromatic region. Compared with the corresponding protonated ligands (H₂L), the signals for the ligands coordinated to an Al^{III} ion were shifted to higher fields (Figure 3). Lyčka et al., demonstrated an octahedral coordination for the homoleptic 1:2 Al^{III} complex with an azp derivative ligand by both the solid-state and solution-state NMR spectroscopy and also observed a similar higher-field shift [42]. The present observations suggest that all the Al^{III} complexes **1** and **2** retained the homoleptic octahedral coordination structure in solution.

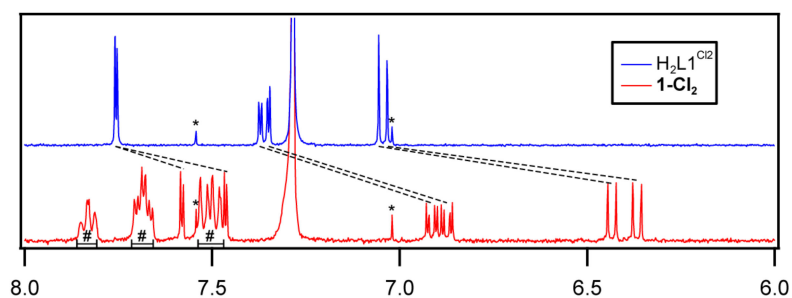


Figure 3. ^1H NMR spectra in the range of 8–6 ppm for ligand $\text{H}_2\text{L1}^{\text{Cl}_2}$ and Al^{III} complex 1-Cl_2 in chloroform- d . * indicates spinning sidebands. # indicates signals from the TPP cation.

2.4. Cyclic Voltammetry (CV)

To investigate the redox properties of the homoleptic 1:2 Al^{III} complexes **1** and **2**, the cyclic voltammograms were recorded at a scan speed of 100 mV s^{-1} in a 0.1 M Bu_4NPF_6 solution of dichloromethane. The voltammograms for all the complexes are shown in Figures 4, S1 and S2. The redox potentials are summarized in Table 2.

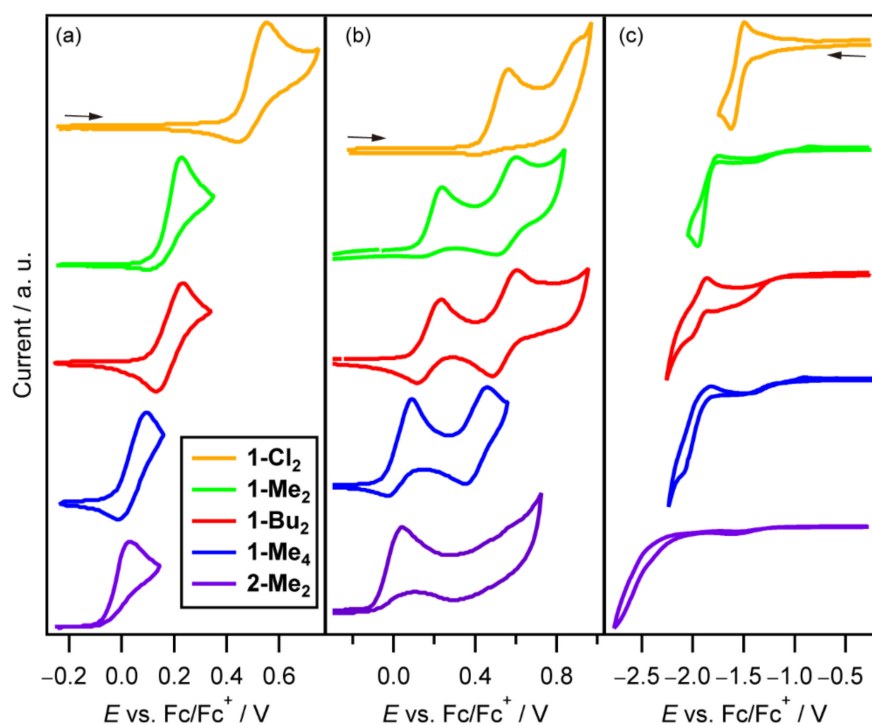


Figure 4. Cyclic voltammograms of the Al^{III} complexes **1** and **2** in a 0.1 M Bu_4NPF_6 solution of dichloromethane. The scan speed was 100 mV s^{-1} . (a) The anodic scans in the range of the first oxidation waves; (b) The anodic scans in the range of the first and second oxidation waves; (c) The cathodic scans in the range of the first reduction waves.

Table 2. Redox potentials ^a (V vs. Fc/Fc^+) for the Al^{III} complexes **1** and **2**.

Complex	E_{pa}	E_{red1} E_{pc}	$E_{1/2}^{\text{b}}$	E_{pa}	E_{ox1} E_{pc}	$E_{1/2}^{\text{b}}$	E_{pa}	E_{ox2} E_{pc}	$E_{1/2}^{\text{b}}$
1-Cl₂	−1.50	−1.62	−1.56	0.57	0.40 ^c	0.49	0.90 ^d	—	—
1-Me₂	−1.73 ^c	−1.96	—	0.24	0.11	0.18	0.60	0.50	0.55
1-Bu₂	−1.86	−1.98 ^d	—	0.24	0.12	0.18	0.61	0.49	0.55
1-Me₄	−1.82	−2.07 ^d	—	0.09	−0.03	0.03	0.46	0.35	0.41
2-Me₂	—	—	—	0.04	—	—	—	—	—

^a The scan speed was 100 mV s^{-1} . ^b $E_{\text{mid}} = (E_{\text{pa}} + E_{\text{pc}})/2$. ^c Broad peak. ^d Shoulder peak.

All the azp complexes **1** showed two partially reversible oxidation waves (Figure 4a,b). Although two or three additional oxidation waves were observed in the further anodic scan (Figure S1), the reduction waves coupled to the first and second oxidation waves for **1-Cl₂** and **1-Me₂** disappeared after the anodic scan potentials exceeded the third oxidation waves. A comparison of the first oxidation peak potentials of the Al^{III} complexes **1** in Table 2 clearly shows the presence of the substitution effect. On the other hand, the reversibility of the oxidative processes varies from one complex to the others. The reduction wave coupled to the first oxidation wave was almost absent in **1-Me₂**, whereas the peak currents of the reduction wave were larger on increasing either the size or the number of substituents in the alkyl-substituted complexes. These observations suggest that the irreversibility of the wave is associated with the reactivity of the oxidation species rather than from the dissociation of coordination bonds.

In the cathodic scan, only **1-Cl₂** showed a reversible and an additional partially reversible reduction ($E_{pa} = -1.81$ (shoulder peak), $E_{pc} = -1.95$ V vs. Fc/Fc⁺) waves, whereas the other azp complexes showed a partially reversible reduction wave in the measurable range (Figure 4c and Figure S1). The substitution effect on the first reduction peak was also observed in **1**.

The imino complex **2-Me₂** exhibited a partially reversible oxidation wave, which accompanied the deposition of an orange film on the working electrode (Figure 4a,b). Although two or three additional oxidation waves were observed in the further anodic scan (Figure S1), these three oxidation waves disappeared in the second and subsequent anodic scans. On the other hand, there was no reduction wave in the cathodic scan in the measurable range (Figure 4c). The anodic shift of the first oxidation peak from **2-Me₂** to **1-Me₂** by 0.20 V suggests that the electronegativity of an azo group was higher than that of an imino group. On the other hand, the oxidation species of the azp ligand complexes **1** were more stable than those of the imino derivative complex **2**.

Although the cyclic voltammograms were recorded in the presence of an equivalent mole of ferrocene (Figure S2), the number of electrons for the oxidation and reduction waves cannot be determined.

2.5. Density Functional Theory Calculations

To give an insight into the origin of the redox waves and the difference in redox behavior between the Al^{III} complexes **1** and **2**, the density functional theory (DFT) calculations in the presence of CH₂Cl₂ were carried out for [Al^{III}(L)₂] anions except for the [Al^{III}(L1^{Bu2})₂] anion, which is expected to give a similar result to the [Al^{III}(L1^{Me2})₂] anion. All the Al^{III} complexes anions could be fully optimized using the polarizable continuum model (PCM) [46]. The energy levels of frontier molecular orbitals (MOs) are listed in Table 3. The frontier molecular orbitals for the [Al^{III}(L1^{Me2})₂] and [Al^{III}(L2^{Me2})₂] anions are shown in Figure 5.

Table 3. Energy levels of frontier molecular orbitals of the Al^{III} complex anions (eV).

Anion	LUMO+1	LUMO	HOMO	HOMO−1
[Al ^{III} (L1 ^{Cl2}) ₂]	−2.527	−2.720	−5.339	−5.343
[Al ^{III} (L1 ^{Me2}) ₂]	−2.132	−2.324	−4.946	−4.953
[Al ^{III} (L1 ^{Me4}) ₂]	−2.025	−2.223	−4.836	−4.839
[Al ^{III} (L2 ^{Me2}) ₂]	−1.562	−1.742	−4.762	−4.763

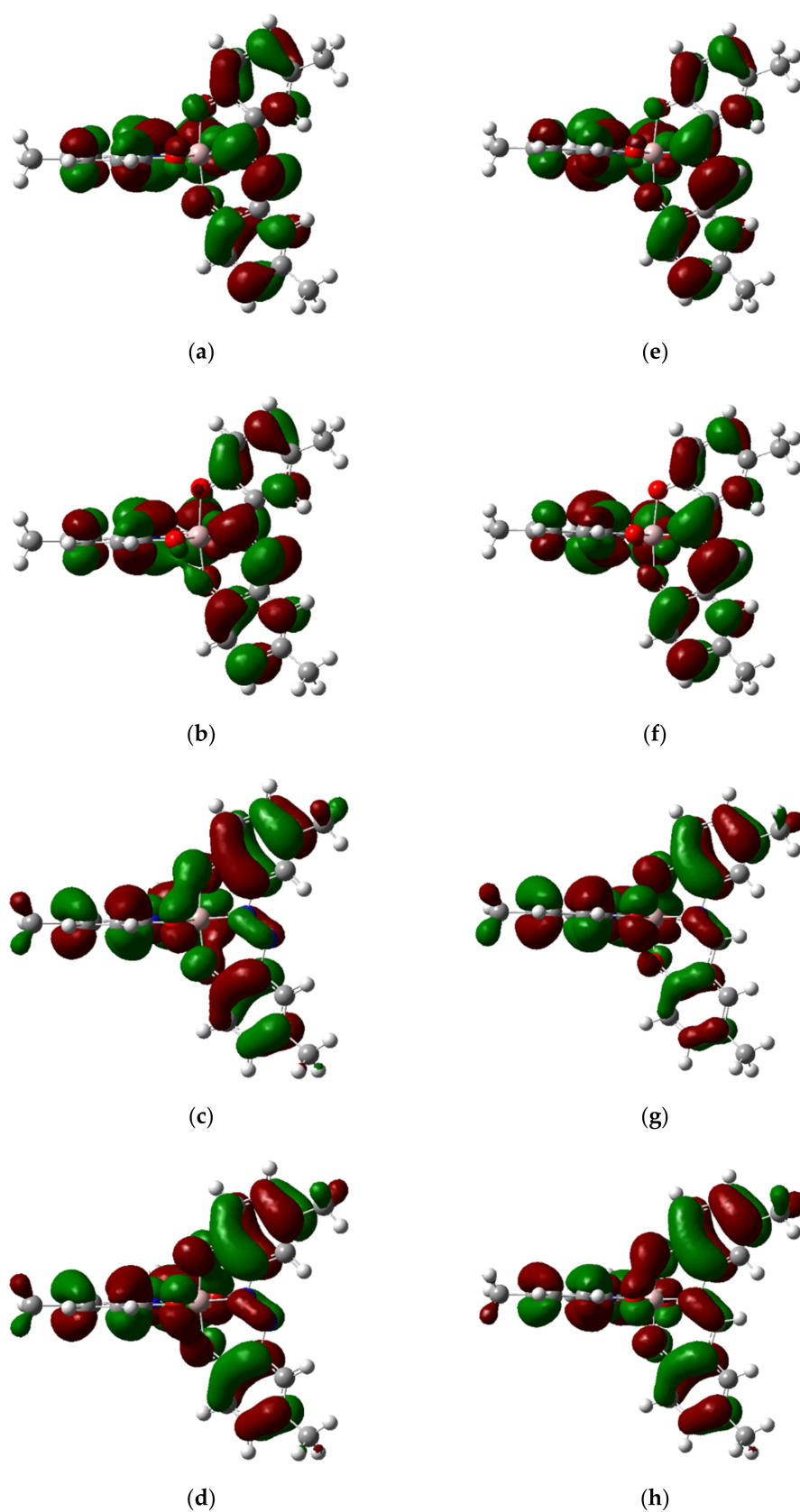


Figure 5. Molecular orbital surfaces. (a) The LUMO+1 of $[\text{Al}^{\text{III}}(\text{L1}^{\text{Me2}})_2]^-$; (b) The LUMO of $[\text{Al}^{\text{III}}(\text{L1}^{\text{Me2}})_2]^-$; (c) The HOMO of $[\text{Al}^{\text{III}}(\text{L1}^{\text{Me2}})_2]^-$; (d) The HOMO−1 of $[\text{Al}^{\text{III}}(\text{L1}^{\text{Me2}})_2]^-$; (e) The LUMO+1 of $[\text{Al}^{\text{III}}(\text{L2}^{\text{Me2}})_2]^-$; (f) The LUMO of $[\text{Al}^{\text{III}}(\text{L2}^{\text{Me2}})_2]^-$; (g) The HOMO of $[\text{Al}^{\text{III}}(\text{L2}^{\text{Me2}})_2]^-$; (h) The HOMO−1 of $[\text{Al}^{\text{III}}(\text{L2}^{\text{Me2}})_2]^-$.

The distribution of MO coefficients for the frontier orbitals was similar in all the Al^{III} anions. The frontier MOs had no MO coefficients on the aluminum atoms as anticipated. In all calculations, the HOMO had larger coefficients on the phenyl rings, whereas the LUMO had larger coefficients on the azo or imino group. The energy levels of HOMO and LUMO were nearly degenerate with those of the HOMO−1 and LUMO+1, respectively. The difference between HOMO and HOMO−1 and between the LUMO and LUMO+1 was that the MO coefficients of one ligand were inverted (Figure 5). The correlation plots between the first oxidation peak potential and the HOMO energy and between the first reduction peak potential and the LUMO energy are shown in Figure 6. These two plots each show an almost linear correlation between the orbital energy and peak potential, which indicates that the first oxidation and first reduction arise from the HOMO and LUMO, respectively.

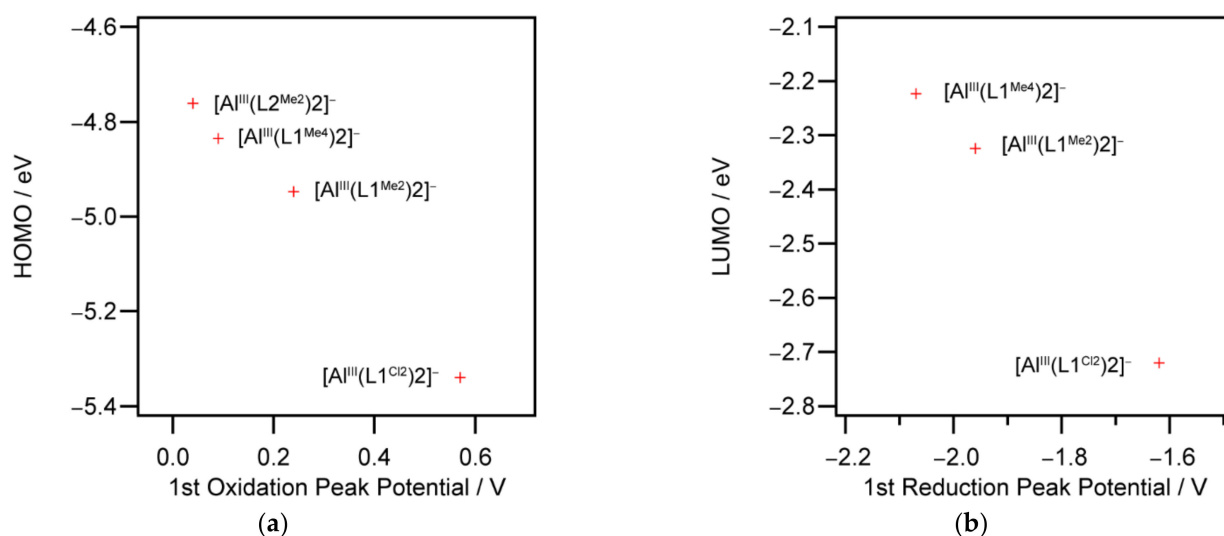


Figure 6. The correlation plots between the HOMO and the first oxidation peak potential (a) and between the LUMO and the first reduction peak potential (b).

As the neutral one-electron oxidative derivatives were optimized under vacuum using the DFT method, the coefficient distributions of the SOMOs for **1-Me₂** and **2-Me₂** were almost the same as those of the corresponding HOMOs (Figure S3). Moreover, the SOMO distributions of two phenolate moieties of the azp ligand were also similar to those of a semiquinone radical reported in the literature [47]. These imply that the oxidation of the azp ligands may form a semiquinone-like radical.

The difference in the distribution of MO coefficients between $[\text{Al}^{\text{III}}(\text{L}1^{\text{Me}2})_2]$ and $[\text{Al}^{\text{III}}(\text{L}2^{\text{Me}2})_2]$ anions is small, but the MO coefficients on the phenyl ring bonded with the nitrogen on the imino group were larger than those bonded with the carbon atom on the imino group in $[\text{Al}^{\text{III}}(\text{L}2^{\text{Me}2})_2]$ anion. This may result in the difference in the stability against oxidation between $[\text{Al}^{\text{III}}(\text{L}1^{\text{Me}2})_2]$ and $[\text{Al}^{\text{III}}(\text{L}2^{\text{Me}2})_2]$ anions.

3. Materials and Methods

3.1. Synthesis

All the chemicals were purchased and used without further purifications. 2-Methoxyanilines **3c** and **3d** were prepared by methylation followed by reduction reactions of corresponding nitrophenols.

3.1.1. General Synthetic Procedure of (2'-Methoxyphenylazo)-2-Hydroxybenzene Derivatives 5

A solution of 2-methoxyanilines **3a–d** (36.5 mmol) in 50 mL of water and 9.4 mL of conc. HCl was stirred and cooled to 0 °C. A solution of NaNO_2 (2.77 g, 40 mmol) in 7 mL of water was added dropwise to the solution. The mixture solution turned to be yellowish-

orange and kept below 5 °C. After confirming the existence of HNO₂ using a KI-starch paper, the solution was quickly transferred to a solution of phenols **4a–d** (35.5 mmol) in 25 mL of an aqueous solution of NaOH (2.92 g, 72.9 mmol). The resulting suspension was stirred for 1 h below 5 °C and then warmed to room temperature. To this suspension was added 2 mL of 3.5% HCl and stirred. The precipitate was filtered and dried in vacuo.

5,5'-Dichloro-2-hydroxy-2'-methoxyazobenzene (5a): 3.0 g of **3a** and 2.0 mL of **4a** were used. Recrystallization from ethyl acetate gave **5a** (2.3 g, 41%) as dark red needles. ¹H NMR (400 MHz, CDCl₃) δ 13.19 (s, 1H), 7.94 (d, *J* = 2.6 Hz, 1H), 7.84 (d, *J* = 2.6 Hz, 1H), 7.43 (dd, *J* = 8.6, 2.6 Hz, 1H), 7.29 (dd, *J* = 8.6, 2.6 Hz, 1H), 7.04 (d, *J* = 8.9 Hz, 1H), 6.99 (d, *J* = 8.8 Hz, 1H), 4.01 (s, 3H) ppm.

5,5'-Dimethyl-2-hydroxy-2'-methoxyazobenzene (5b): 5.0 g of **3b** (36.5 mmol) and 3.8 g of **4b** (35.5 mmol) were used. Recrystallization from ethyl acetate gave **5b** (4.8 g, 51%) as orange crystals. ¹H NMR (400 MHz, CDCl₃) δ 13.46 (s, 1H), 7.74 (d, *J* = 1.6 Hz, 1H), 7.66 (d, *J* = 1.7 Hz, 1H), 7.26 (dd, *J* = 8.4, 2.3 Hz, 1H), 7.13 (dd, *J* = 8.4, 2.2 Hz, 1H), 6.98 (d, *J* = 8.5 Hz, 1H), 6.93 (d, *J* = 8.4 Hz, 1H), 3.97 (s, 3H), 2.38 (s, 3H), 2.36 (s, 3H) ppm.

5,5'-Di-*t*-butyl-2-hydroxy-2'-methoxyazobenzene (5c): 0.55 g of **3c** (3.1 mmol) and 0.44 g of **4c** (3.1 mmol) were used. Recrystallization from ethyl acetate gave **5c** (0.42 g, 41%) as orange crystals. ¹H NMR (400 MHz, CDCl₃) δ 13.58 (s, 1H), 7.97 (d, *J* = 2.5 Hz, 1H), 7.90 (d, *J* = 2.5 Hz, 1H), 7.50 (dd, *J* = 8.7, 2.5 Hz, 1H), 7.37 (dd, *J* = 8.7, 2.5 Hz, 1H), 7.02 (d, *J* = 8.7 Hz, 1H), 6.97 (d, *J* = 8.7 Hz, 1H), 3.99 (s, 3H), 1.39 (s, 9H), 1.37 (s, 9H) ppm.

3,3',5,5'-tetramethyl-2-hydroxy-2'-methoxyazobenzene (5d): 0.92 g of **3d** (6.1 mmol) and 0.73 mL of **4d** (6.1 mmol) were used. Recrystallization from ethyl acetate gave **5d** (1.3 g, 75%) as orange crystals. ¹H NMR (400 MHz, CDCl₃) δ 13.54 (s, 1H), 7.59 (m, 1H), 7.48 (m, 1H), 7.12 (m, 1H), 7.06 (m, 1H), 3.91 (s, 3H), 2.35 (s, 6H), 2.34 (s, 3H), 2.29 (s, 3H) ppm.

3.1.2. General Synthetic Procedure of 2,2'-Dihydroxyazobenzene (H₂azp) Derivatives H₂L1

A finely powdered AlCl₃ (73.4 mmol) was added portionwise to a stirred solution of **5** (18.3 mmol) in 75 mL of chloroform. The resulting red suspension was warmed to 30 °C and then 38 mL of pyridine was added dropwise to this suspension. The mixture was heated to reflux for 2 h and then cooled to room temperature. The mixture was poured into 150 mL of ice water and then acidified by adding 30 mL of 36% HCl. After evaporating chloroform, the mixture was heated at 80 °C for two hours. The resulting precipitate was filtered and dried in vacuo.

5,5'-Dichloro-2,2'-dihydroxyazobenzene (H₂L1^{Cl2}): H₂L1^{Cl2} was synthesized using 2.0 g of **5a**. Recrystallization from ethyl acetate gave H₂L1^{Cl2} as orange crystals (1.1 g, 56%). ¹H NMR (400 MHz, CDCl₃) δ 11.90 (s, 2H), 7.73 (d, *J* = 2.6 Hz, 2H), 7.34 (dd, *J* = 2.6, 8.9 Hz, 2H), 7.02 (d, *J* = 8.9 Hz, 2H), ppm.

5,5'-Dimethyl-2,2'-dihydroxyazobenzene (H₂L1^{Me2}): H₂L1^{Me2} was synthesized using 4.7 g of **5b**. Recrystallization from ethyl acetate gave H₂L1^{Me2} as orange crystals (3.3 g, 74%). ¹H NMR (400 MHz, CDCl₃) δ 12.14 (s, 2H), 7.51 (d, *J* = 1.4 Hz, 2H), 7.16 (dd, *J* = 8.4, 2.1 Hz, 2H), 6.94 (d, *J* = 8.4 Hz, 2H), 2.38 (s, 6H) ppm.

5,5'-Di-*t*-butyl-2,2'-dihydroxyazobenzene (H₂L1^{Bu2}): H₂L1^{Bu2} was synthesized using 0.42 g of **5c**. Recrystallization from ethyl acetate gave H₂L1^{Bu2} as orange crystals (0.28 g, 70%). ¹H NMR (400 MHz, CDCl₃) δ 12.28 (s, 2H), 7.67 (d, *J* = 2.4 Hz, 2H), 7.41 (dd, *J* = 8.7, 2.5 Hz, 2H), 7.00 (d, *J* = 8.7 Hz, 2H), 1.36 (s, 18H) ppm.

3,3',5,5'-Tetramethyl-2,2'-dihydroxyazobenzene (H₂L1^{Me4}): H₂L1^{Me4} was synthesized using 1.3 g of **5d**. Recrystallization from ethyl acetate gave H₂L1^{Me4} as orange crystals (0.78 g, 66%). ¹H NMR (400 MHz, CDCl₃) δ 12.55 (s, 2H), 7.34 (s, 2H), 7.05 (s, 2H), 2.33 (s, 6H), 2.28 (s, 6H) ppm. Anal. Calcd. for C₁₆H₁₈N₂O₂: C, 71.09; H, 6.71; N, 10.36%. Found: C, 71.03; H, 6.72; N, 10.32%.

3.1.3. Synthetic Procedure of N-(2-Hydroxy-5-Methylphenyl)-5-Methylsalicylaldimine (H_2L^{Me2})

2-amino-4-methylphenol (1.0 g, 8.1 mmol) and 2-hydroxy-5-methylbenzaldehyde (1.1 g, 8.1 mmol) were dissolved in 25 mL of methanol. The solution was heated to reflux and stirred for 2 h. The solution was cooled to room temperature. The orange precipitate was filtered and dried. (2.4 g, 51%). 1H NMR (400 MHz, $CDCl_3$) δ 12.08 (s, 2H), 8.63 (s, 1H), 7.23–7.21 (m, 2H), 7.01 (d, J = 8.2, 1.5 Hz, 1H), 6.95–6.93 (m, 2H), 6.91 (d, J = 8.2 Hz, 1H), 2.335 (s, 3H), 2.327 (s, 3H) ppm.

3.1.4. General Synthetic Procedure of the $[Al^{III}(L1)_2]$ (1) and $[Al^{III}(L2)_2]$ (2) Complexes

A 28% methanol solution of sodium methoxide (4.0 mmol) was added dropwise to a suspension of H_2L1 or H_2L2 (0.74 mmol) in 10 mL of methanol. The suspension was heated to 60 °C and stirred for 20 min to become a dark solution. A solution of $Al(NO_3)_3 \cdot 9H_2O$ (0.37 mmol) in 9 mL of methanol was added to the solution and then heated to reflux for 2 h. Tetraphenylphosphonium bromide salts (0.93 mmol) in 15 mL of methanol were added to the solution and then stirred for 30 min. After evaporating the solution to a few mL, water was added. The precipitate was filtered and washed with water and dried in vacuo.

$TPP[Al^{III}(L1^{Cl2})_2] \cdot H_2O$ (**1-Cl₂**· H_2O): **1-Cl₂** was synthesized using 200 mg of H_2L1^{Cl2} . Recrystallization of the crude salt from dichloromethane-hexane gave 238 mg (73%) as dark purple needles. The elemental analysis was performed using an air-dried sample. 1H NMR (400 MHz, $CDCl_3$) δ 7.83–7.79 (m, 4H), 7.68–7.63 (m, 8H), 7.56 (d, J = 2.7 Hz, 2H), 7.51–7.46 (m, 8H), 7.44 (d, J = 2.8 Hz, 2H), 6.89 (dd, J = 8.9, 2.7 Hz, 2H), 6.85 (dd, J = 9.1, 2.9 Hz, 2H), 6.41 (d, J = 8.9 Hz, 2H), 6.34 (d, J = 9.0 Hz, 2H) ppm. Anal. Calcd. for $C_{48}H_{34}AlCl_4N_4O_5P$: C, 60.91; H, 3.62; N, 5.92%. Found: C, 61.01; H, 3.60; N, 5.96%.

$TPP[Al^{III}(L1^{Me2})_2] \cdot CH_3OH \cdot H_2O$ (**1-Me₂**· $CH_3OH \cdot H_2O$): **1-Me₂** was synthesized using 100 mg of H_2L1^{Me2} . In total, 170 mg of crude salt was obtained (46%). Recrystallization of the crude salt from methanol-diethyl ether gave dark purple thin rectangles. 1H NMR (400 MHz, $CDCl_3$) δ 7.76–7.72 (m, 4H), 7.63–7.59 (m, 8H), 7.45–7.41 (m, 12H), 6.68 (dd, J = 8.6, 2.3 Hz, 2H), 6.64 (dd, J = 8.7, 2.6 Hz, 2H), 6.29 (d, J = 8.4 Hz, 2H), 6.21 (d, J = 8.6 Hz, 2H), 2.14 (s, 6H), 2.12 (s, 6H) ppm. Anal. Calcd. For $C_{53}H_{50}AlN_4O_6P$: C, 70.97; H, 5.62; N, 6.25%. Found: C, 70.69; H, 5.55; N, 6.16%.

$TPP[Al^{III}(L1^{Bu2})_2]$ (**1-Bu₂**): **1-Bu₂** was synthesized using 200 mg of H_2L1^{Bu2} . Recrystallization of the crude TPP salt from acetonitrile-diethyl ether gave 255 mg (82%) as dark red platelets. 1H NMR (400 MHz, $DMSO-d_6$) δ 7.99–7.94 (m, 4H), 7.84–7.79 (m, 8H), 7.77–7.71 (m, 8H), 7.65 (d, J = 2.5 Hz, 2H), 7.52 (d, J = 2.7 Hz, 2H), 7.21 (dd, J = 8.8 Hz, 2.6 Hz, 2H), 7.18 (dd, J = 8.9 Hz, 2.7 Hz, 2H), 6.35 (d, J = 8.8 Hz, 4H), 1.29 (s, 18H), 1.28 (s, 18H) ppm. 1H NMR (400 MHz, $CDCl_3$) δ 7.74–7.71 (m, 4H), 7.73 (d, J = 2.5 Hz, 2H), 7.62–7.57 (m, 8H), 7.54 (d, J = 2.7 Hz, 2H), 7.48–7.43 (m, 8H), 6.93 (dd, J = 8.9 Hz, 2.6 Hz, 2H), 6.90 (dd, J = 8.9 Hz, 2.8 Hz, 2H), 6.33 (d, J = 8.7 Hz, 2H), 6.23 (d, J = 8.8 Hz, 2H), 1.23 (s, 18H), 1.22 (s, 18H) ppm. Anal. Calcd. for $C_{64}H_{68}AlN_4O_4P$: C, 75.72; H, 6.75; N, 5.52%. Found: C, 75.34; H, 6.75; N, 5.88%.

$TPP[Al^{III}(L1^{Me4})_2] \cdot 1.5H_2O$ (**1-Me₄**· $1.5H_2O$): **1-Me₄** was synthesized using 200 mg of H_2L1^{Me4} . Recrystallization of the crude salt from acetonitrile-diethyl ether gave 231 mg (69%) as dark red platelets. 1H NMR (400 MHz, $DMSO-d_6$) δ 7.99–7.94 (m, 4H), 7.84–7.79 (m, 8H), 7.77–7.71 (m, 8H), 7.27 (d, J = 2.1 Hz, 2H), 7.20 (d, J = 2.3 Hz, 2H), 6.81 (d, J = 2.0 Hz, 2H), 6.79 (d, J = 2.2 Hz, 2H), 2.18 (s, 6H), 2.17 (s, 6H), 1.81 (s, 6H), 1.58 (s, 6H) ppm. 1H NMR (400 MHz, $CDCl_3$) δ 7.74–7.70 (m, 4H), 7.63–7.58 (m, 8H), 7.45–7.40 (m, 8H), 7.26 (the signal overlapped with that of $CHCl_3$, 2H), 7.13 (d, J = 2.1 Hz, 2H), 6.62 (d, J = 1.7 Hz, 4H), 2.15 (s, 6H), 2.13 (s, 6H), 1.65 (s, 6H), 1.50 (s, 6H) ppm. Anal. Calcd. for $C_{56}H_{55}AlN_4O_{5.5}P$: C, 72.32; H, 5.96; N, 6.02%. Found: C, 72.14; H, 5.94; N, 6.21%.

$TPP[Al^{III}(L2^{Me2})_2]$ (**2-Me₂**): **2-Me₂** was synthesized using 200 mg of H_2L2^{Me2} . Recrystallization of the crude salt from acetonitrile-diethyl ether gave 204 mg (58%) as orange needles. The elemental analysis was performed using an air-dried sample. 1H NMR (400 MHz, $CDCl_3$) δ 8.37 (s, 2H), 7.77–7.74 (m, 4H), 7.66–7.61 (m, 8H), 7.48–7.43 (m, 8H),

7.00 (d, $J = 1.6$ Hz, 2H), 6.85 (d, $J = 2.1$ Hz, 2H), 6.72 (dd, $J = 8.5, 2.2$ Hz, 2H), 6.47 (dd, $J = 8.3, 1.7$ Hz, 2H), 6.26 (d, $J = 8.5$ Hz, 2H), 6.22 (d, $J = 8.2$ Hz, 2H), 2.11 (s, 6H), 2.11(s, 6H) ppm. Anal. Calcd. For $C_{58}H_{52}AlN_4O_4P$: C, 76.76; H, 5.49; N, 3.32%. Found: C, 76.79; H, 5.34; N, 3.37%.

3.2. Physical Measurements

Cyclic voltammograms were recorded using an Ivium Technologies CompactStat.h standard electrochemical interface. Platinum wires were used as working and counter electrodes. A BAS RE-7 nonaqueous reference electrode (Ag/Ag^+) was used as a reference electrode. A few mg of the Al complexes were dissolved in a 0.1 M Bu_4NPF_6 solution of dichloromethane. A ferrocene was used as an internal reference and the potential axis was corrected by the half-wave potential of Fc/Fc^+ .

3.3. Crystal Structure Determinations

A crystal was mounted in a polyimide loop. A nitrogen gas flow temperature controller was used for the temperature variable measurements. All data were collected on a Bruker APEX II CCD area detector with monochromated Mo- $K\alpha$ radiation generated by a Bruker Turbo X-ray Source coupled with Helios multilayer optics. All data collections and calculations were performed using the APEX2 crystallographic software package (Bruker AXS). The data were collected to a maximum 2θ value of 55.0° . A total of 720 oscillation images were collected. The APEX3 crystallographic software package (Bruker AXS) was used to determine the unit cell parameters and for data collection. Data were integrated using SAINT. Numerical absorption correction was applied using SADABS. The structures at all temperatures were solved by direct methods and refined by full-matrix least-squares methods based on F^2 using the SHELXTL program. During the refinements, the azp ligands in all the Al complexes except **1-Cl₂** were found to be orientationally disordered. The structures and temperature factors for the disordered azp ligands were restrained. During the refinements for **1-Cl₂**, the solvent molecules could not be refined properly and an inversion twin was detected. Thus, the SQUEEZE procedure [48] was applied and the twin volume fractions were refined using TWIN and BASF commands. All non-hydrogen atoms were refined anisotropically. Hydrogen atoms were generated by calculation and refined using the riding model. CCDC 2156173–2156177 contains the supplementary crystallographic data for this paper. These data can be obtained free of charge via <http://www.ccdc.cam.ac.uk/conts/retrieving.html> (or from the CCDC, 12 Union Road, Cambridge, UK).

3.4. DFT Calculations

The geometry optimized calculations for the Al^{III} complex anions and the neutral Al^{III} complexes were performed at the B3LYP level [49,50] using the Gaussian 16 program package [51]. The 6-311+G(d,p) basis set for H, C, O, N [52,53], and Al [54–56] atoms were used. The atomic coordinates for the $[Al^{III}(L1^{Me2})_2]$ anion were taken from the main component of the disordered ligands in the crystal structure of **1-Me₂**. The atomic coordinates for the other aluminum anions were generated from the corresponding substitutions of the optimized $[Al^{III}(L1^{Me2})_2]$ anion. After the geometry optimization under vacuum, the geometry optimization calculations in the presence of CH_2Cl_2 were performed using the polarizable continuum model (PCM) [47]. No imaginary frequencies were found in the optimized structures. Cartesian coordinates of all Al^{III} complex anions calculated by the B3LYP level of theory are summarized in Tables S1–S4 (Supplementary Materials). The geometry optimizations for the neutral one-electron oxidative Al^{III} complex species under vacuum were performed using the atomic coordinates of the optimized $[Al^{III}(L1^{Me2})_2]$ and $[Al^{III}(L2^{Me2})_2]$ anions under vacuum. No imaginary frequencies were found in the optimized structures. Cartesian coordinates of the neutral Al^{III} complexes $[Al^{III}(L1^{Me2})_2]$ and $[Al^{III}(L2^{Me2})_2]$ calculated by the B3LYP level of theory are summarized in Tables S5 and S6.

4. Conclusions

We report the improved procedure of obtaining the H₂azp derivatives with electron-donating and electron-withdrawing substituents, and the preparations and structural characterizations of the homoleptic 1:2 Al^{III} complexes with the azp ligands and imino derivative. The ligand-centered oxidations in the homoleptic 1:2 Al^{III} complexes with the azp ligands in solution were confirmed by the ¹H NMR spectroscopy, cyclic voltammetry, and DFT calculation. The present result revealed that a semiquinone-like radical can be generated by the oxidation reaction of an azp derivative and thus the azp derivatives are a redox-active ligand in either the reduction or oxidation direction. Since the azp ligands are more stable than the imino derivative ligand under oxidative conditions, the introduction of appropriate substituents to the azp ligand and the combination with an appropriate metal ion can lead to the possibility that the metal azp complex exhibits valence tautomerism or electron-transfer-induced magnetic transitions. Further investigation toward this goal is now in progress.

Supplementary Materials: The following are available online at <https://www.mdpi.com/article/10.3390/inorganics10060084/s1>, Figure S1: Cyclic voltammograms in the full potential range of the cathodic and anodic scans; Figure S2: Cyclic voltammograms in the presence of an equivalent mole of ferrocene; Figure S3: Molecular orbital surfaces of the SOMOs; Table S1: Crystallographic data for the Al^{III} complexes 1 and 2; Table S2: Cartesian coordinates of the [Al^{III}(L¹Cl²)₂] anion; Table S3: Cartesian coordinates of the [Al^{III}(L¹Me²)₂] anion; Table S4: Cartesian coordinates of the [Al^{III}(L¹Me⁴)₂] anion; Table S5: Cartesian coordinates of the [Al^{III}(L²Me²)₂] anion; Table S6: Cartesian coordinates of the neutral [Al^{III}(L¹Me²)₂] complex; Table S7: Cartesian coordinates of the neutral [Al^{III}(L²Me²)₂] complex.

Author Contributions: Conceptualization, K.T.; methodology, K.T.; validation, T.N., K.U., A.M. and S.M.; formal analysis, T.N., K.U., A.M. and S.M.; investigation, T.N., K.U., A.M. and S.M.; resources, K.T.; data curation, K.T.; writing—original draft preparation, K.T.; writing—review and editing, K.T.; visualization, K.T. and T.N.; supervision, K.T.; project administration, K.T.; funding acquisition, K.T. All authors have read and agreed to the published version of the manuscript.

Funding: This research was partially funded by a Grant-in-Aid for Scientific Research (C) (No. 19K05402) from the Ministry of Education, Culture, Sports, Science, and Technology of Japan, a grant from the CASIO Science Promotion Foundation, and a grant from Hyogo Science and Technology Association.

Institutional Review Board Statement: Not applicable.

Informed Consent Statement: Not applicable.

Data Availability Statement: The crystallographic data can be obtained free of charge via <http://www.ccdc.cam.ac.uk/conts/retrieving.html> (or from the CCDC, 12 Union Road, Cambridge CB2 1EZ, UK; Fax: +44 1223 336033; E-mail: deposit@ccdc.cam.ac.uk).

Acknowledgments: K.T. is grateful to T. Osakai and K. Eda at Kobe University for the discussion on electrochemistry and DFT calculation. K.T. is thankful to M. Lemaire at Brock University for reading the manuscript and suggesting the revision. K.T. thanks Y. Furuie at Kobe University for performing the elemental analysis.

Conflicts of Interest: The authors declare no conflict of interest.

References

1. Tezgerevska, T.; Alley, K.G.; Boskovic, C. Valence Tautomerism in Metal Complexes: Stimulated and Reversible Intramolecular Electron Transfer between Metal Centers and Organic Ligands. *Coord. Chem. Rev.* **2014**, *268*, 23–40. [CrossRef]
2. Motokawa, N.; Miyasaka, H.; Yamashita, M.; Dunbar, K.R. An Electron-Transfer Ferromagnet with T_c = 107 K Based on a Three-Dimensional [Ru₂]₂/TCNQ System. *Angew. Chem. Int. Ed.* **2008**, *47*, 7760–7763. [CrossRef]
3. Kato, R. Conductive Copper Salts of 2,5-Disubstituted N,N'-Dicyanobenzoquinonediimines (DCNQIs): Structural and Physical Properties. *Bull. Chem. Soc. Jpn.* **2000**, *73*, 515–534. [CrossRef]
4. Freeman, D.C.; White, C.E. The Structure and Characteristics of the Fluorescent Metal Chelates of o,o'-Dihydroxyazo Compounds 1. *J. Am. Chem. Soc.* **1956**, *78*, 2678–2682. [CrossRef]
5. Diehl, H.; Ellingboe, J. Azo Dyes as Indicators for Calcium and Magnesium. *Anal. Chem.* **1960**, *32*, 1120–1123. [CrossRef]

6. Diehl, H.; Olsen, R.; Spielholtz, G.I.; Jensen, R. Fluorometric and Spectrophotometric Determination of Magnesium with o,o'-Dihydroxyazobenzene. *Anal. Chem.* **1963**, *35*, 1144–1154. [[CrossRef](#)]
7. Knoeck, J.; Buchholz, J.A. Structure, Bonding, and Fluorescence of Bivalent Metal Chelates of o,o'-Dihydroxyazobenzene. *Talanta* **1971**, *18*, 895–903. [[CrossRef](#)]
8. Kirby, J.R.; Milburn, R.M.; Saylor, J.H. A Spectrophotometric Study of o,o'-Dihydroxyazobenzene and Its Chelates with Aluminum, Gallium and Indium. *Anal. Chim. Acta* **1962**, *26*, 458–469. [[CrossRef](#)]
9. Hiraki, K. Metal Chelates of Aromatic o,o'-Dihydroxyazo Compounds. I. The Fluorescence Properties of the Metal Chelates of o,o'-Dihydroxyazobenzene and Their Use in Fluorometry. *Bull. Chem. Soc. Jpn.* **1973**, *46*, 2438–2443. [[CrossRef](#)]
10. Hoshino, H.; Yotsuyanagi, T. Highly Selective Determination of Trace Metal Ions with 2,2'-Dihydroxyazobenzene by Ion-Pair Reversed-Phase Partition HPLC-Spectrophotometric Detection System. *Chem. Lett.* **1984**, *13*, 1445–1448. [[CrossRef](#)]
11. Schetty, G. Über Die Räumliche Anordnung von 1:2-Metallkomplexfarbstoffen Der Azo- Und Azomethin-Reihe. *Helv. Chim. Acta* **1962**, *45*, 1095–1102. [[CrossRef](#)]
12. Schetty, G. Die Sterische Anordnung Der 1:2-Metallkomplexfarbstoffe Im Lichte Der Geometrischen Gegebenheiten. *Helv. Chim. Acta* **1963**, *46*, 1132–1143. [[CrossRef](#)]
13. Schetty, G. Neuartige Isomeriefälle Bei 1:2-Cr^{III}- Und Co^{III}-Komplexen von o, o'-Dihydroxyazoverbindungen: Pyramidal Gebundener Stickstoff Mit Hoher Inversionsbarriere? *Helv. Chim. Acta* **1970**, *53*, 1437–1459. [[CrossRef](#)]
14. Schetty, G.; Steiner, E. Untersuchungen Der Symmetrieverhältnisse in Äquatorial Koordinierten 2:1-Arylazo-Co^{III}-Komplexen Mit Hilfe Der Protonenresonanz. *Helv. Chim. Acta* **1972**, *55*, 1509–1532. [[CrossRef](#)]
15. Schetty, G.; Steiner, E. Die Aufklärung Der Isomerie-Ursachen Bei Äquatorial Koordinierten 2:1-Arylazo-Co(III)-Komplexen Mit Hilfe Der Kernmagnetischen Protonenresonanz. *Helv. Chim. Acta* **1974**, *57*, 2149–2172. [[CrossRef](#)]
16. Schetty, G. Zur Frage Der Existenz Isomerer, Äquatorial Koordinierter 1:2-Co(III)-Komplexe Aus Symmetrischen o,o'-Dihydroxyazofarbstoffen. *Helv. Chim. Acta* **1975**, *58*, 377–380. [[CrossRef](#)]
17. Grieb, R.; Niggli, A. Die Strukturen Zweier 1:2-Chromkomplexe Von o,o'-Dihydroxydiaryl-Trans-Azo-Farbstoffmolekeln. *Helv. Chim. Acta* **1965**, *48*, 317–320. [[CrossRef](#)]
18. Dutta, S.; Basu, P.; Chakravorty, A. Mononuclear Manganese(IV) in Tridentate ONO Coordination. Synthesis, Structure, and Redox Regulation via Oxygen Donor Variation. *Inorg. Chem.* **1991**, *30*, 4031–4037. [[CrossRef](#)]
19. Hefele, H.; Ludwig, E.; Uhlemann, E.; Nöth, H. Titan(IV)-Komplexe Mit Dreizähligen Diaciden Liganden. Kristallstruktur von Bis [2,6-Diphenacylpyridinato(2-)]Titan(IV). *Z. Anorg. Allg. Chem.* **1995**, *621*, 1431–1435. [[CrossRef](#)]
20. Hefele, H.; Jancke, H.; Sawusch, S.; Schilde, U.; Uhlemann, E. ¹³C-CP/MAS-NMR Spectroscopy of Tridentate Diacidic Ligands and Their Titanium(IV) Chelates. Molecular Structure of Bis[Benzoylacetone Thiobenzoylhydrazonato(2-)]Titanium(IV). *Struct. Chem.* **1997**, *8*, 211–216. [[CrossRef](#)]
21. Sanna, D.; Várnagy, K.; Lihi, N.; Micera, G.; Garribba, E. Formation of New Non-Oxido Vanadium(IV) Species in Aqueous Solution and in the Solid State by Tridentate (O, N, O) Ligands and Rationalization of Their EPR Behavior. *Inorg. Chem.* **2013**, *52*, 8202–8213. [[CrossRef](#)] [[PubMed](#)]
22. Yoshikawa, Y.; Sakurai, H.; Crans, D.C.; Micera, G.; Garribba, E. Structural and Redox Requirements for the Action of Anti-Diabetic Vanadium Compounds. *Dalton Trans.* **2014**, *43*, 6965–6972. [[CrossRef](#)] [[PubMed](#)]
23. Sanna, D.; Sciortino, G.; Ugone, V.; Micera, G.; Garribba, E. Nonoxido VIV Complexes: Prediction of the EPR Spectrum and Electronic Structure of Simple Coordination Compounds and Amavadin. *Inorg. Chem.* **2016**, *55*, 7373–7387. [[CrossRef](#)] [[PubMed](#)]
24. Dutta, S.; Chakravorty, A. Water Soluble Manganese(III) and Manganese(IV) Complexes of Tridentate Ono Ligands. *Polyhedron* **1994**, *13*, 1811–1816. [[CrossRef](#)]
25. Evangelio, E.; Saiz-Poseu, J.; Maspocho, D.; Wurst, K.; Busque, F.; Ruiz-Molina, D. Synthesis, X-ray Structure and Reactivity of a Sterically Protected Azobisphenol Ligand: On the Quest for New Multifunctional Active Ligands. *Eur. J. Inorg. Chem.* **2008**, *2008*, 2278–2285. [[CrossRef](#)]
26. Abildgaard, J.; Hansen, P.E.; Josephsen, J.; Lycka, A. Assignment of the Ligating Nitrogen in o,o'-Dihydroxyazoarene Complexes of Nickel-, Palladium-, and Platinum(II) by ¹H and ¹³C NMR Spectroscopy. *Inorg. Chem.* **1994**, *33*, 5271–5277. [[CrossRef](#)]
27. Abildgaard, J.; Hansen, P.E.; Josephsen, J.; Hansen, B.K.V.; Sørensen, H.O.; Larsen, S. Synthesis and Characterization of Nickel-, Palladium- and Platinum(II) Complexes of Three o,o'-Dihydroxydiarylazo Dyes: Determination of the Coordination Geometry of This Comprehensive Series of Tridentate Diaryl Dye Complexes by Combining Results from NM. *Inorg. Chim. Acta* **2006**, *359*, 4493–4502. [[CrossRef](#)]
28. Speier, G.; Csihony, J.; Whalen, A.M.; Pierpont, C.G. Studies on Aerobic Reactions of Ammonia/3,5-Di-Terf-Butylcatechol Schiff-Base Condensation Products with Copper, Copper(I), and Copper(II). Strong Copper(II)-Radical Ferromagnetic Exchange and Observations on a Unique N-N Coupling Reaction. *Inorg. Chem.* **1996**, *35*, 3519–3524. [[CrossRef](#)]
29. Mitra, S.; Biswas, H.; Bandyopadhyay, P. Synthesis, Spectral Properties and Redox Behaviour of Cis-Dioxo-Molybdenum(VI) Complexes with Tridentate Arylazo Ligands. *Polyhedron* **1995**, *14*, 1581–1584. [[CrossRef](#)]
30. Takahashi, K.; Kawamukai, K.; Okai, M.; Mochida, T.; Sakurai, T.; Ohta, H.; Yamamoto, T.; Einaga, Y.; Shiota, Y.; Yoshizawa, K. A New Family of Anionic Fe^{III} Spin Crossover Complexes Featuring a Weak-Field N₂O₄ Coordination Octahedron. *Chem. Eur. J.* **2016**, *22*, 1253–1257. [[CrossRef](#)]

31. Murata, S.; Takahashi, K.; Sakurai, T.; Ohta, H.; Yamamoto, T.; Einaga, Y.; Shiota, Y.; Yoshizawa, K. The Role of Coulomb Interactions for Spin Crossover Behaviors and Crystal Structural Transformation in Novel Anionic Fe(III) Complexes from a π -Extended ONO Ligand. *Crystals* **2016**, *6*, 49. [\[CrossRef\]](#)
32. Murata, S.; Takahashi, K.; Mochida, T.; Sakurai, T.; Ohta, H.; Yamamoto, T.; Einaga, Y. Cooperative Spin-Crossover Transition from Three-Dimensional Purely π -Stacking Interactions in a Neutral Heteroleptic Azobisphenolate Fe^{III} Complex with a N₃O₃ Coordination Sphere. *Dalton Trans.* **2017**, *46*, 5786–5789. [\[CrossRef\]](#) [\[PubMed\]](#)
33. Miyawaki, A.; Mochida, T.; Sakurai, T.; Ohta, H.; Takahashi, K. The Impact of the Next-Nearest Neighbor Dispersion Interactions on Spin Crossover Transition Enthalpy Evidenced by Experimental and Computational Analyses of Neutral π -Extended Heteroleptic Fe(III) Complexes. *Inorg. Chem.* **2020**, *59*, 12295–12303. [\[CrossRef\]](#) [\[PubMed\]](#)
34. Murata, S.; Takahashi, K.; Sakurai, T.; Ohta, H. Single-Crystal-to-Single-Crystal Transformation in Hydrogen-Bond-Induced High-Spin Pseudopolymorphs from Protonated Cation Salts with a π -Extended Spin Crossover Fe(III) Complex Anion. *Polyhedron* **2017**, *136*, 170–175. [\[CrossRef\]](#)
35. Miyawaki, A.; Eda, K.; Mochida, T.; Sakurai, T.; Ohta, H.; Nakajima, T.; Takahashi, K. Spin-Crossover-Triggered Linkage Isomerization by the Pedal-like Motion of the Azobenzene Ligand in a Neutral Heteroleptic Iron(III) Complex. *Inorg. Chem.* **2021**, *60*, 12735–12739. [\[CrossRef\]](#) [\[PubMed\]](#)
36. Phonsri, W.; Lewis, B.A.I.; Jameson, G.N.L.; Murray, K.S. Double Spin Crossovers: A New Double Salt Strategy to Improve Magnetic and Memory Properties. *Chem. Commun.* **2019**, *55*, 14031–14034. [\[CrossRef\]](#)
37. Smékal, Z.; Novák, P.; Zeller, M.; Antal, P.; Čížmár, E.; Herchel, R. Synthesis, Crystal Structure, ⁵⁷Fe Mössbauer Spectroscopy and Magnetic Properties of High-Spin Iron(III) Anionic Complexes [Fe(Azp)₂][−] (H₂azp = 2,2′-Dihydroxyazobenzene) with Organic Cations. *Polyhedron* **2022**, *212*, 115586. [\[CrossRef\]](#)
38. Willard, H.H.; Dean, J.A. Polarographic Determination of Aluminum: Use of an Organic Reagent. *Anal. Chem.* **1950**, *22*, 1264–1267. [\[CrossRef\]](#)
39. Zhang, L.; Liu, Y.; Deng, L. Three-Coordinate Cobalt(IV) and Cobalt(V) Imido Complexes with N-Heterocyclic Carbene Ligation: Synthesis, Structure, and Their Distinct Reactivity in C–H Bond Amination. *J. Am. Chem. Soc.* **2014**, *136*, 15525–15528. [\[CrossRef\]](#)
40. Kwon, Y.M.; Lee, Y.; Evenson, G.E.; Jackson, T.A.; Wang, D. Crystal Structure and C–H Bond-Cleaving Reactivity of a Mononuclear Co^{IV}–Dinitrate Complex. *J. Am. Chem. Soc.* **2020**, *142*, 13435–13441. [\[CrossRef\]](#)
41. Cui, C.; Roesky, H.W.; Schmidt, H.G.; Noltemeyer, M.; Hao, H.; Cimpoesu, F. Synthesis and Structure of a Monomeric Aluminum(I) Compound [(HC(CMeNAr)₂)Al] (Ar = 2,6-IPr₂C₆H₃): A Stable Aluminum Analogue of a Carbene. *Angew. Chem. Int. Ed.* **2000**, *39*, 4274–4276. [\[CrossRef\]](#)
42. Lyčka, A.; Rys, P.; Skrabal, P. ²⁷Al, ¹⁵N, ¹³C and ¹H NMR Spectra of the 2:1 Aluminium(III) Complexes of Some Azo Dyes. *Magn. Reson. Chem.* **1998**, *36*, 279–284. [\[CrossRef\]](#)
43. Freeman, D.C., Jr.; White, C.E. Notes-Preparation of o,o′-Dihydroxyazo Compounds. *J. Org. Chem.* **1956**, *21*, 379. [\[CrossRef\]](#)
44. Hunter, L.; Barnes, R.S. CCLXVII.—Halogen Derivatives of o- and p-Azophenol. *J. Chem. Soc.* **1928**, 2051–2058. [\[CrossRef\]](#)
45. Shannon, R.D. Revised Effective Ionic Radii and Systematic Studies of Interatomic Distances in Halides and Chalcogenides. *Acta Cryst.* **1976**, *A32*, 751–767. [\[CrossRef\]](#)
46. Tomasi, J.; Mennucci, B.; Cammi, R. Quantum mechanical continuum solvation models. *Chem. Rev.* **2005**, *105*, 2999–3093. [\[CrossRef\]](#) [\[PubMed\]](#)
47. Witwicki, M.; Jezierska, J. Effects of solvents, ligand aromaticity, and coordination sphere on the g tensor of anionic o-semiquinone radicals complexed by Mg²⁺ ions: DFT studies. *J. Phys. Chem. B* **2011**, *115*, 3172–3184. [\[CrossRef\]](#)
48. Spek, A.L. PLATON SQUEEZE: A Tool for the Calculation of the Disordered Solvent Contribution to the Calculated Structure Factors. *Acta Cryst. C* **2015**, *71*, 9–18. [\[CrossRef\]](#)
49. Becke, A.D. A New Mixing of Hartree-Fock and Local Density-Functional Theories. *J. Chem. Phys.* **1993**, *98*, 1372–1377. [\[CrossRef\]](#)
50. Lee, C.; Yang, W.; Parr, R.G. Development of the Colle-Salvetti Correlation-Energy Formula into a Functional of the Electron Density. *Phys. Rev. B* **1988**, *37*, 785–789. [\[CrossRef\]](#)
51. Frisch, M.J.; Trucks, G.W.; Schlegel, H.B.; Scuseria, G.E.; Robb, M.A.; Cheeseman, J.R.; Scalmani, G.; Barone, V.; Petersson, G.A.; Nakatsuji, H.; et al. *Gaussian 16*; Revision C.01; Gaussian, Inc.: Wallingford, CT, USA, 2016.
52. Krishnan, R.; Binkley, J.S.; Seeger, R.; Pople, J.A. Self-consistent Molecular Orbital Methods. XX. A Basis Set for Correlated Wave Functions. *J. Chem. Phys.* **1980**, *72*, 650–654. [\[CrossRef\]](#)
53. Clark, T.; Chandrasekhar, J.; Spitznagel, G.W.; Schleyer, P.V.R. Efficient Diffuse Function-Augmented Basis Sets for Anion Calculations. III. The 3-21+G Basis Set for First-Row Elements, Li–F. *J. Comput. Chem.* **1983**, *4*, 294–301. [\[CrossRef\]](#)
54. McLean, A.D.; Chandler, G.S. Contracted Gaussian Basis Sets for Molecular Calculations. I. Second Row Atoms, Z = 11–18. *J. Chem. Phys.* **1980**, *72*, 5639–5648. [\[CrossRef\]](#)
55. Francel, M.M.; Pietro, W.J.; Hehre, W.J.; Binkley, J.S.; Gordon, M.S.; DeFrees, D.J.; Pople, J.A. Self-consistent Molecular Orbital Methods. XXIII. A Polarization-type Basis Set for Second-row Elements. *J. Chem. Phys.* **1982**, *77*, 3654–3665. [\[CrossRef\]](#)
56. Spitznagel, G.W.; Clark, T.; von Ragué Schleyer, P.; Hehre, W.J. An Evaluation of the Performance of Diffuse Function-Augmented Basis Sets for Second Row Elements, Na–Cl. *J. Comput. Chem.* **1987**, *8*, 1109–1111. [\[CrossRef\]](#)